

Article

Wear Resistance Evaluation of Self-Fluxing Nickel-Based Coating Deposited on AISI 4340 Steel by Atmospheric Plasma Spray

Francisco C. Monção¹, Felipe R. Caliarì², Filipe E. Freitas³, Antônio A. Couto¹ , Arnaldo Augusto¹, Carlos R. C. Lima^{1,*}  and Marcos Massi¹

¹ School of Engineering, Mackenzie Presbyterian University, São Paulo 01302-907, Brazil; francisco.moncao@vulkan.com (F.C.M.); marcos.massi@mackenzie.br (M.M.)

² Center for Thermal Spray Research, Stony Brook University, Stony Brook, NY 11794-2275, USA

³ Anton Paar do Brasil Ltda., São Paulo 04026-090, Brazil; filipefreitas@antonpaar.com.br

* Correspondence: carlos.lima@mackenzie.br

Abstract: Materials with enhanced wear resistance are constantly in high demand. Nickel-based self-fluxing materials deposited by atmospheric plasma spraying (APS) have feasible wear resistance performance. This study aimed to evaluate the results of a nickel-based self-fluxing alloy coating deposited on AISI 4340 steel substrate using APS. Additionally, the temperature at which the remelting process achieved optimal results was investigated. The AISI 4340 steel substrate samples were coated with a self-fluxing NiCrBSiCFe powder by APS. The post-coating remelting process was performed in a controlled atmosphere tube furnace at 900, 1000, and 1100 °C. Microstructural analysis was carried out by Scanning Electron Microscopy (SEM) before and after remelting. The estimated porosity of the as-sprayed sample was 3.28%, while the remelted coating sample at 1100 °C had only 0.22% porosity. Furthermore, a microhardness measurement was conducted, and the best condition yielded an average value of 750 HV_{0.5}. Tribological tests were performed to evaluate the coefficient of friction and wear rates, revealing that at 1100 °C, the as-sprayed coating had a wear rate of 9.16×10^{-5} [mm³/(N*m)] and the remelted coating had 4.106×10^{-5} [mm³/(N*m)]. The wear-loss volume was determined to be 14.1 mm³ for the as-sprayed coating sample and 3.6 mm³ for the remelted coating at 1100 °C.



Citation: Monção, F.C.; Caliarì, F.R.; Freitas, F.E.; Couto, A.A.; Augusto, A.; Lima, C.R.C.; Massi, M. Wear Resistance Evaluation of Self-Fluxing Nickel-Based Coating Deposited on AISI 4340 Steel by Atmospheric Plasma Spray. *Metals* **2024**, *14*, 532. <https://doi.org/10.3390/met14050532>

Academic Editor: Sima A. Alidokht

Received: 24 March 2024

Revised: 25 April 2024

Accepted: 28 April 2024

Published: 30 April 2024



Copyright: © 2024 by the authors. Licensee MDPI, Basel, Switzerland. This article is an open access article distributed under the terms and conditions of the Creative Commons Attribution (CC BY) license (<https://creativecommons.org/licenses/by/4.0/>).

Keywords: atmospheric plasma spray; nickel-based self-fluxing coating; post-process coating remelting; hardness; wear resistance

1. Introduction

The demand for materials with good wear resistance has been increasing, especially in the industrial sector, which is always looking for cost reductions to make it more competitive. This demand affects all categories of the industrial sector that use machinery parts with sliding or rotating movements, including energy, mining, and steelmaking. To meet this demand, the development and availability of materials with enhanced tribological properties are necessary [1–4]. According to Holmberg and Erdemir [5], between 15% and 20% of the world's energy consumption in the industrial sector is influenced by the wear rate of machinery parts. Furthermore, approximately 20% of all energy produced worldwide is used for overcoming the friction generated between parts of machines and equipment, which strongly justifies investments in research and development in tribology [5]. In 1966, a study by Jost [6] led him to conclude that between 1.0 and 1.40% of the Gross Domestic Product in an industrialized country could be saved by the introduction of the best tribological practices.

A good example of standard materials with attractive properties is AISI 4340 steel, which is a heat-treatable low-alloy steel containing chromium, nickel, and molybdenum. After the heat treatments of quenching and tempering, this steel can exhibit a favorable

combination of high strength and toughness as well as good hardenability and fatigue resistance, enabling its use in a wide range of applications in sectors, such as aerospace, automotive, and industrial machinery and equipment [7–13]. However, for applications where parts are exposed to harsh environments, especially with abrasive contaminants, this steel, with only conventional heat treatments, is not resistant enough to withstand such conditions, leading to degradation and losses.

The development of coatings with enhanced wear resistance deposited on the surfaces of steel by different techniques, such as thermal spray, has expanded its ability to fulfill the demands and expectations of industrial applications. Thermal spray is a group of processes by which metallic or non-metallic coating materials are deposited. The material particles are kinetically energized by a jet, which makes them impinge the substrate surface, cooling rapidly and forming a solid splat. This cycle is continuously repeated until the desired coating thickness is obtained. This process is very versatile in the deposition of coatings, as it can deposit coatings on practically any part size and any type of material.

Among thermal spray processes, atmospheric plasma spraying (APS) is a highly feasible option to efficiently protect the material against accelerated wear and tear. It is also economically viable, especially in large parts with high added value. This process basically consists of thermal plasmas produced by direct current (DC) arc or by radio frequency discharges as heat sources in the deposition, allowing high torch temperatures that provide coatings with excellent densities, excellent cohesion, and relatively low porosity [1,14,15].

The coating powder material selected and applied in this work was a nickel-based self-fluxing alloy. It has good wear resistance, operation at high temperatures, corrosion resistance, and self-fluxing characteristics. Self-fluxing alloys have been developed based on metallurgical refining theory to achieve oxide-free coatings by post-spray fusing process. The addition of B and Si elements into the nickel alloy improves the fluxing properties, acting as deoxidizers, forming borosilicate, protecting the main alloying element against oxidation, and lowering the melting temperature (together with chromium) of pure nickel [16,17].

Furthermore, APS can significantly contribute to the circular economy, which is a model of production and consumption involving sharing, renting, reusing, repairing, refurbishing, and recycling existing materials and products for as long as possible. When the life cycle of products is extended, there is less waste, which helps provide sustainability and promotes economic benefits. McGinty [18] reported that, from more than 100 billion tons of materials resources that enter the global economy every year, only 8.6% are recycled to be used again. He also reported that the use of materials resources has tripled since 1970 and could double by 2050 if we continue to practice the linear economy, i.e., business as usual. APS process can contribute directly to repairing and refurbishing parts that have suffered wearing and/or corrosion. This means that instead of discarding machinery parts and components, they can be reused and not generate waste by increasing the life of the substrate materials of these components, thus reducing the need for additional materials [19].

This work aims to evaluate the influence of the remelting temperature on the tribological behavior of plasma-sprayed Ni-based self-fluxing alloy coating. The novelty of this research is to determine the best limit for the remelting temperature of the Ni-based self-fluxing coating in a controlled atmosphere furnace to enhance the wear resistance. We also evaluated the influence of the remelting temperature on the microstructure morphology, roughness, microhardness, and porosity.

2. Materials and Methods

In this section, we provide a detailed explanation of the materials, equipment, and methods that were used in the experiments of this research. The first step involved machining the samples, followed by measuring their hardness and roughness. Once this initial step was complete, the samples were coated with a nickel-based self-fluxing alloy using atmospheric plasma spraying, which was then followed by a remelting heat treatment. To

assess the quality of the coatings, we conducted microstructural analysis using a scanning electron microscope (SEM), as well as tests for microhardness, roughness, and tribology.

2.1. Substrate Material, Sample Machining, Coating Material, and Deposition

AISI 4340 rolled-steel samples were used as a substrate, whose chemical composition is shown in Table 1. Samples with a diameter of 20 × 3 mm thick and 20 × 20 × 5 mm thick were machined in a CNC machining center with 5 axes and double pallets, Mazak variaxis 630-5X II (Mazak, Florence, KY, USA). The feedstock powder used in the experiments was a commercial self-fluxing nickel-based material, Diamalloy 2001 (Oerlikon Metco, Westbury, NY, USA), with a particle size distribution in the range of −45 to +15 μm with a spheroidal morphology, which facilitates the free-flowing material feed during the coating deposition. Additionally, this powder is produced by the gas atomization process, which assures a homogeneous and consistent alloy, contributing to a high-quality coating level. The chemical composition of the self-fluxing powder is presented in Table 2. The coatings were deposited using the Plasma Spray System AT-3000 with SG-100 torch, Thermach (Appleton, WI, USA). The spraying parameters are shown in Table 3.

Table 1. Chemical composition of the AISI 4340 rolled steel (wt.%).

C	Mn	Si	Ni	Cr	Mo
0.38–0.43	0.60–0.80	0.15–0.35	1.65–2.00	0.70–0.90	0.20–0.30

Table 2. Chemical composition of the Self-fluxing alloy powder Diamalloy 2001 (wt.%).

Ni	Cr	B	Si	C	Fe
Balance	17	3.5	4	1	4

Table 3. Process parameters of the atmospheric plasma spray.

Parameter Description	Value
Argon flow rate (SLPM)	53
Hydrogen flow rate (SLPM)	1.6
Carrier gas flow (SLPM)	2.8
Current (A)	750
Voltage (V)	60
Spraying Velocity (mm/s)	300
Standoff Distance (mm)	100
Nozzle diameter (mm)	6.7
Cooling pressure (bar)	3–5
Surface temperature (°C)	≈300

2.2. Coating Remelting Process

The remelting heat treatment of the coated samples was performed at three temperature levels, 900, 1000, and 1100 °C, with a heating rate of 10.7 °C/min. The criteria for selecting the remelting temperatures were based on the manufacturer’s datasheet for the coating material. The datasheet stated that the coating material can be fused in a temperature range of 1035 to 1065 °C. Some examples of remelting temperatures found in the literature did not exceed 1050 °C, particularly when the remelting process was not performed in a vacuum furnace [16,20]. Given this information, it was decided to establish 1000 °C as the central reference value for the remelting temperature, with a variation of ±100 °C for conducting the experiments. The best value for the heating rate found in the literature, without intermediate levels, was 10.7 °C/min. This slow heating rate was chosen to ensure the elimination of most possible impurities on the sample surface before reaching the melting peak, with a low risk of sample distortions. The samples were kept for 20 min at each melting peak temperature to ensure proper material soaking. A very low cooling

rate of 2 °C/minute was also established to prevent any internal stress in the samples. Figure 1 presents the remelted heat treatment cycle. For this heat treatment, a Jung tube furnace LT 3212 was used, with a maximum temperature of 1200 °C.

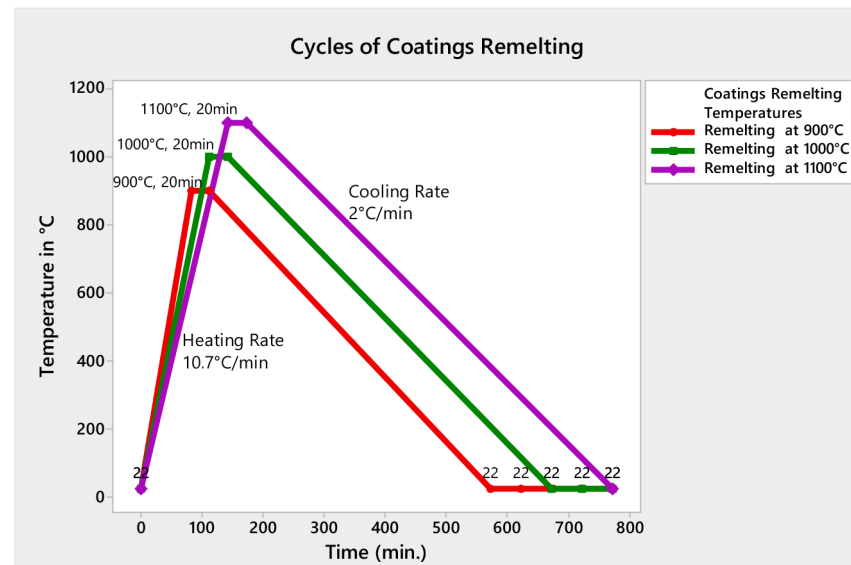


Figure 1. Controlled atmosphere tube furnace heat/cooling cycle.

2.3. Microstructural Analysis, Porosity Estimation, Roughness Measurement, and Microhardness Measurement

The microstructural examination of the morphology of the coatings was carried out using a Jeol Scanning Electron Microscope, JSM-6510 (JEOL, Peabody, MA, USA), with a coupled EDS module. The SEM images were obtained from Secondary Electrons at an operating voltage of 25 KV. The porosity of the coating was estimated by sampling five different regions from SEM micrographs, using the open-source image analysis software ImageJ (Version 1.54d) to obtain the average percent of porosity. The roughness Ra measurement was performed using the roughness measurement device Mitutoyo, model 2 SJ-219 (Mitutoyo, Jundiaí, Brazil), with a resolution of 0.006 μm in five different regions on each sample. To measure the microhardness, a hardness tester, EMCO-Test, Zwick-Roell (Kuchl, Salzburg, Austria), was used with a load of 0.5 kg ($\text{HV}_{0.5}$).

2.4. Tribological Tests

Tribological tests were performed on the coatings to determine the coefficient of friction (CoF) and wear rate under different conditions, i.e., as-sprayed coating and remelted coatings at 900, 1000, and 1100 °C, using Anton Paar ball-on-plate Tribometer TRB3 (Anton Paar, Ashland, VA, USA) with the parameters given in Table 4.

Table 4. Tribological tests parameters.

Static Partner			Load	Environmental Conditions			F. Amp. Stroke	Freq.	Cycles
Geometry	Dimension	Material		Temp.	Humidity	Atmosphere			
Ball	ϕ 6.00 mm	Al_2O_3	20 N	25 °C	60%	Air	10 mm	4 Hz	5000

2.5. Wear Test

To determine the wear in this work, the criteria established in the standard ASTM G133-05 (2016) [21] adopted were related to Linearly Reciprocating Ball-on-Flat Sliding Wear. According to this standard, the main quantities of interest are the wear volume of the

contacting ball and the flat specimen lost material. The flat specimen wear track volume is computed by multiplying the average cross-sectional worn area ($W_{q, avg}$) with the sliding stroke (s), according to Equation (1).

$$W_{v, flat} = W_{q, avg} \times S \quad (1)$$

where: $W_{v, flat}$ is the lost volume of the flat specimen in mm^3 .

$W_{q, avg}$ is the average cross-sectional worn area in mm^2 .

S is the length of the sliding stroke in mm.

To measure and calculate the average cross-sectional worn area by the standard, the first three profiles are taken to measure its area. A variation between them of less than 25% indicates a homogenous wear track and is considered efficient, which happened in this study.

To calculate the cross-sectional worn area and its average, the open-source image analysis software ImageJ (Version 1.54d) was used again.

3. Results and Discussion

3.1. Microstructural Analysis

Figure 2 shows the micrographs obtained by Scanning Electron Microscopy (SEM) from cross-sections of the as-sprayed coatings and coatings remelted at 900, 1000, and 1100 °C. The different morphology of each coating condition was influenced by the remelting temperatures or as sprayed. Comparing the as-sprayed coating and the remelted coating at 1100 °C illustrates the contrast between the morphologies. The as-sprayed coating exhibits many pores, voids, and unmelted particles. On the other hand, the remelted coating at 1100 °C has no voids, no unmelted particles, and practically no pores. The observed precipitates in the cross-section of the remelted coating at 1100 °C were due to the supersaturation during the thermal treatment. This temperature level is borderline for remelting in a non-vacuum furnace for this kind of coating. Kazamer et al. [20] reported that based on thermal analysis of a similar coating powder applied in this work, the remelting temperature limit is 1075 °C; thus, they decided to remelt at 1050 °C. In a study on the effect of high temperature of the heat treatment to remelt Ni-based coating, Bergant et al. [22] deposited low-carbon steel using the flame-spraying process and concluded that the highest temperature to obtain the lowest porosity percentage on the coating as well as the best wear and corrosion resistance was 1080 °C. Kim et al. [23] reported that for Ni-based self-fluxing coatings, when melting and fluxing happen, the liquid phase provides shiny, smooth surfaces but remains in the solid phase to provide the stiffness necessary to keep from forming the semi-molten deposit. This narrow window is the limit to evaluate properties, especially the tribological property of wear.

Another important thing observed in the micrographs is the effect of the Inter-lamellar interface. First, even with the great scientific advances in the developments of processes and technologies in 112 years of existence, thermal spray metal coatings generally present a lamellar structure packed by multiple flattened splats, which hampers the quality of the bonding between coating and substrate, as many factors can affect the bonding results, including impurities, substrate roughness, substrate, and coating temperatures. However, notice on the micrographs that the effect of the Inter-lamellar decreased as the coating remelting temperature increased until it was no longer noticeable. In Figure 2a, the bonding quality of the as-sprayed coating is not good. Figure 2b shows the remelted coating at 900 °C in which the effect of the Inter-lamellar interface remains pronounced. In Figure 2c of the remelted coating at 1000 °C, the Inter-lamellar interface effect has been significantly reduced. Finally, in Figure 2d, the remelted coating at 1100 °C exhibits no effects of the Inter-lamellar interface [24].

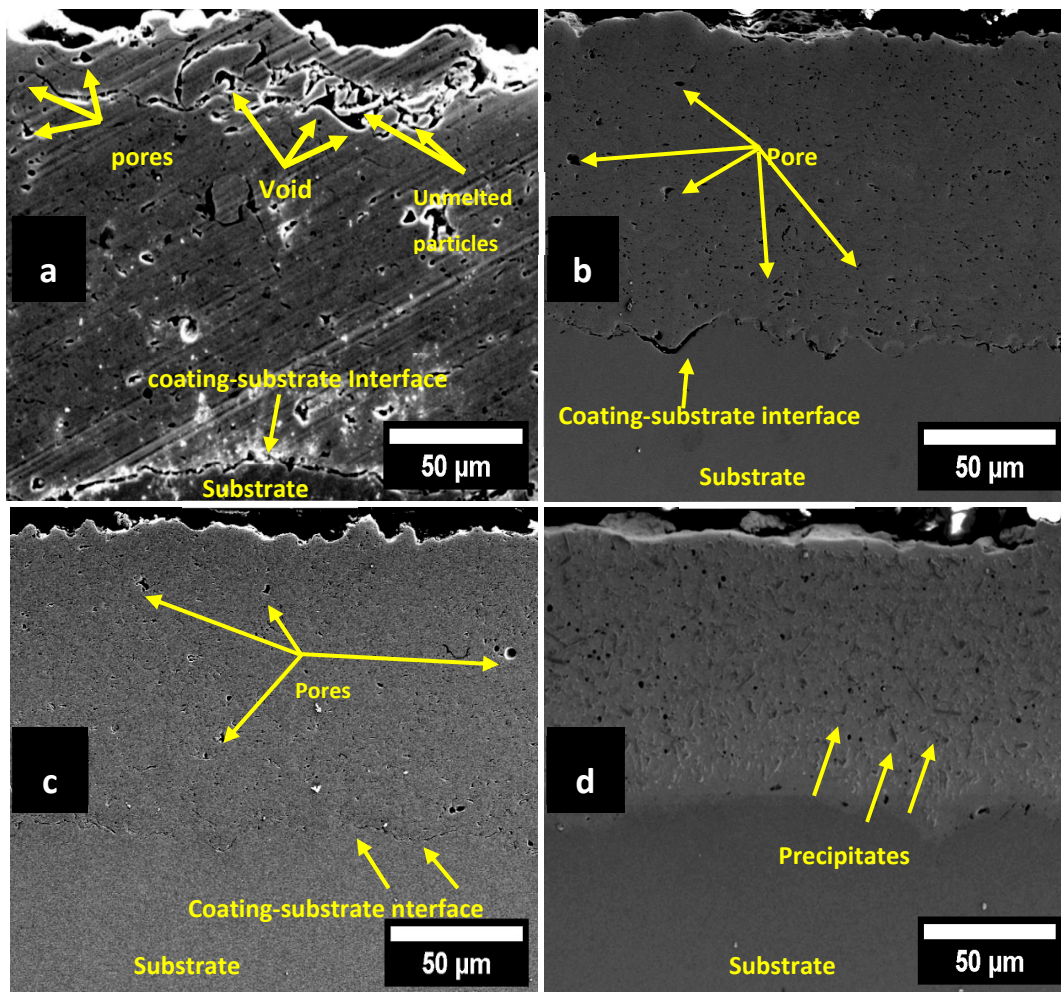


Figure 2. SEM micrographs of coatings cross-sections. (a) As sprayed, (b) remelted coating at 900 °C, (c) remelted coating at 1000 °C, (d) remelted coating at 1100 °C.

3.2. Coatings Porosity Percentage of the Total Coating Sample Area

The density of porosity, presented in Figure 3a–d, is highlighted by the red marks and shows the calculated average percentage of porosity. The average porosity percentage of the coatings was determined in an area of 28,900 μm^2 ($170 \times 170 \mu\text{m}$), selected in three samples for each remelting condition, totaling an area of 86,700 μm^2 for each condition. In this area, the average percentage of porosity was estimated.

There was a strong relationship between the coating remelting temperature and the percentage of porosity. The percentage of porosity of the as-sprayed coating (Figure 3a) and the coating remelted at 1100 °C (Figure 3d) has a ratio of 15. This means that the coating remelted at 1100 °C has a percentage of porosity 15 times less than the porosity of the as-sprayed coating. The porosities obtained in this work are completely satisfactory, as the percentage of porosity for the as-sprayed coating tended to reach the best value reported in the literature and on the industrial market. Odhiambo et al. [25] reported that the normal range of porosity for the Plasma Spray process is between 3% and 8%, while this research obtained 3.28%. The best value after remelting found by Kornienko et al. [1] with a similar coating material was 0.96% porosity, while our best porosity was 0.22%.

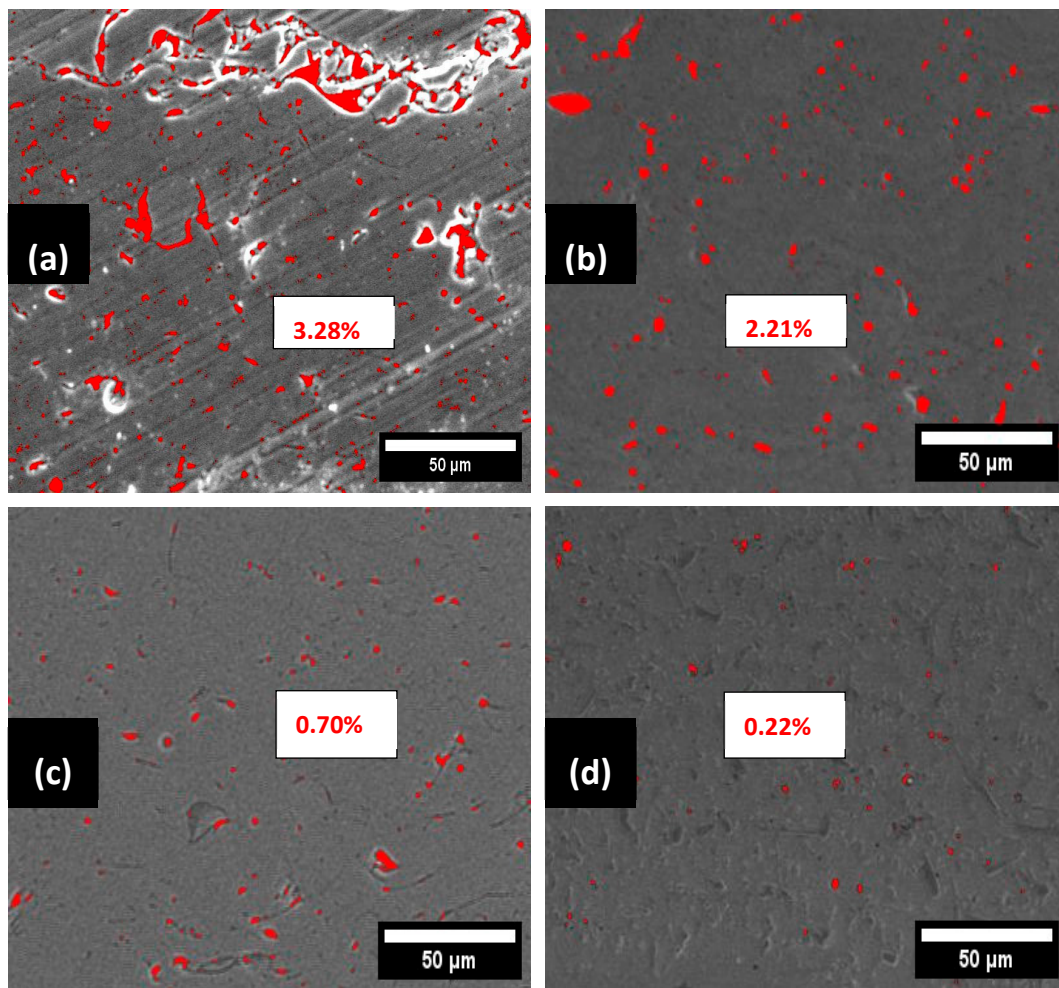


Figure 3. SEM micrographs of coating cross-sections highlighting the density and percentage of porosity from each sample coating area. (a) As-sprayed, (b) remelted coating at 900 °C, (c) remelted coating at 1000 °C, (d) remelted coating at 1100 °C.

3.3. Tribological Test Results: Coefficient of Friction, Wear Rate, Wear Track, and Lost Volume

The tribological behavior of the coatings was first evaluated by the coefficient of friction (CoF). At the beginning of the tribological test, the CoF curve in Figure 4 indicates instability for all sample conditions. However, the amplitude of this instability depends on the topographic characteristics of the sample surface, such as the roughness profile, porosities, and density. The CoF curves of the as-sprayed and remelted samples at 1100 °C exhibit a significant difference in the amplitude of the curve. The curve of the remelted sample at 1100 °C is much smoother. This happened because the surface of this sample (remelted at 1100 °C) is smoother due to lower roughness, much less porosity, and higher density. The stability for all samples occurred after around 250 cycles. After that, the CoF was approximately 0.45 for the remelted sample at 1100 °C, around 0.56 for the as-sprayed sample, 0.50 for the remelted samples at 900 °C, and 0.48 for the sample at 1000 °C. Compared to several relatively similar cases reported in the literature, these CoF results align with or, in some cases, are even better than previous results. Nevertheless, comparing the CoF is not always simple because small variability in a sample can mean a substantial difference in the CoF result [26–28].

The wear rate in Figure 5 was significantly influenced by the coating remelt temperature. The wear rate of the as-sprayed sample, which was 9.16×10^{-5} [mm³/(N*m)], was 2.23 times higher than that of the remelted at 1100 °C sample, which was 4.106×10^{-5} [mm³/(N*m)]. The wear rate decreases 1.82 times in the sample remelted at 1100 °C versus the one

remelted at 900 °C, and comparing the sample remelted at 1100 °C with the one at 1000 °C, this relation decreases even more, reaching 1.46 times. The enhanced wear resistance of the coating, which is seen as a direct function of the increase in its remelting temperature, leads to several factors that together enhance wear resistance, including the densification of the coating that influences the reduction in its porosity and topography, consequently reducing the roughness profile. Furthermore, during the remelting process, more homogeneous second phases are formed (carbides and borides) that contribute to hardening and enhanced wear resistance. The same approach and similar results are found in the literature [28–30].

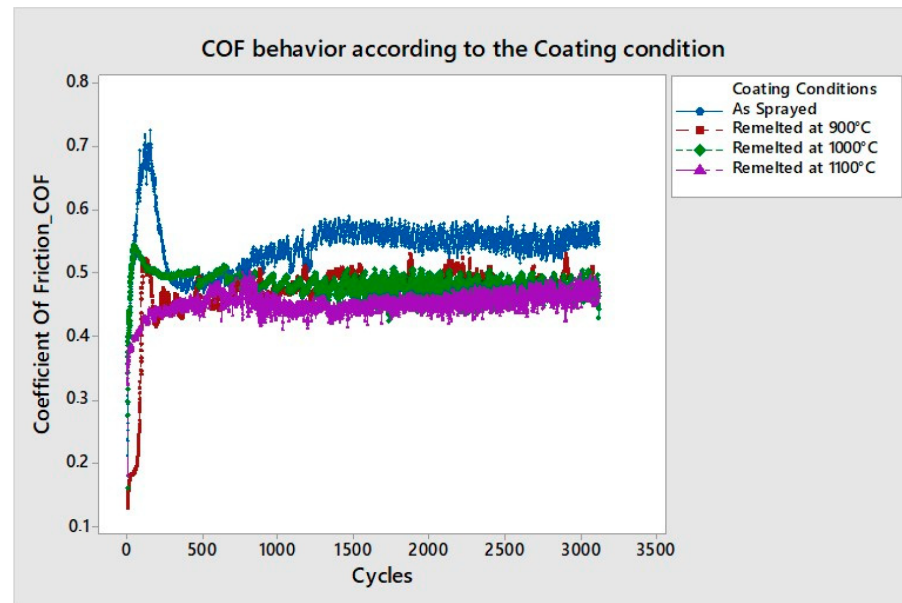


Figure 4. Coefficient of friction of the As-sprayed, remelted coating at 900 °C, remelted coating at 1000 °C, and remelted coating at 1100 °C.

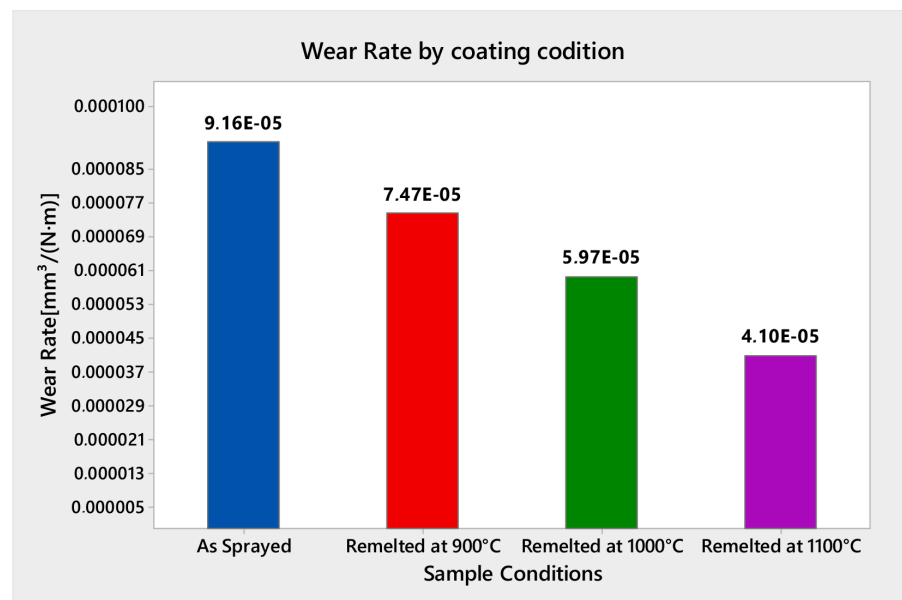


Figure 5. Wear rate by each sample coating condition.

Also pertaining to the results of the tribological behavior of the samples, the consequences of wear can be quantified to predict the useful life of the sample so this procedure can be replicated in the manufacturing environment. One of the simplest ways is by calculating the wear-lost volume of the coating. The tribological test provides important

information, such as wear track and length of sliding stroke, which can be used to calculate the wear loss volume. Figure 6 and Table 5 present the wear tracks for each sample condition as well as their calculated area results. Using these results and the length of the sliding stroke, it was calculated according to the standard ASTM G133-05 (2016) [20], and the results are provided in Table 5. In Figure 7, the track profiles and lost areas demonstrate that the wear resistance of coatings is strongly influenced by their remelted temperature.

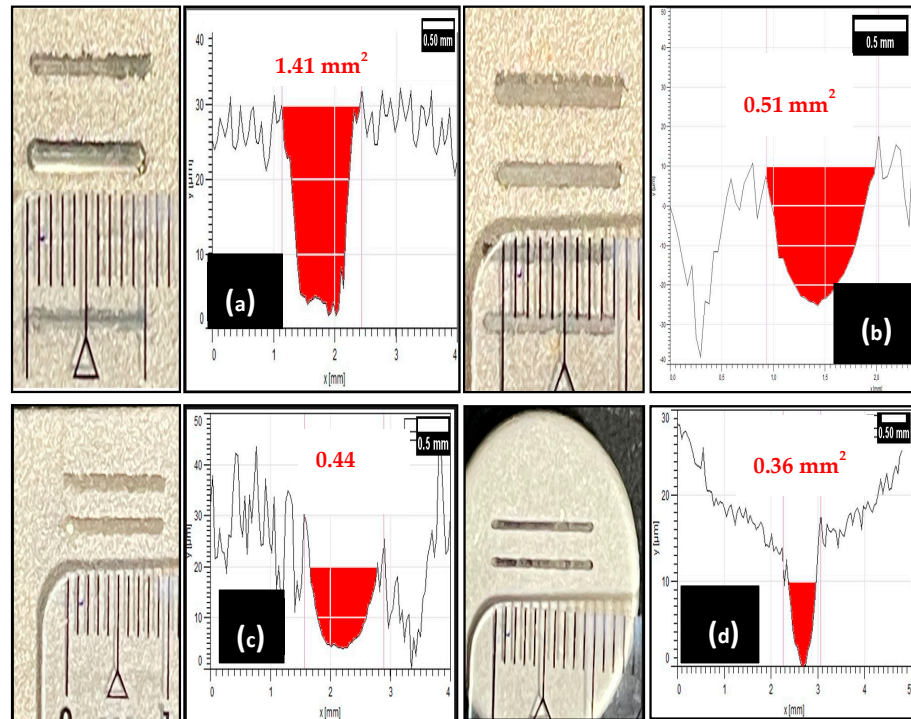


Figure 6. Wear track after Linearly Reciprocating Ball-on-Flat Sliding Test on coating sample condition: (a) as-sprayed, (b) remelted coating at 900 °C, (c) remelted coating at 1000 °C, (d) remelted coating at 1100 °C.

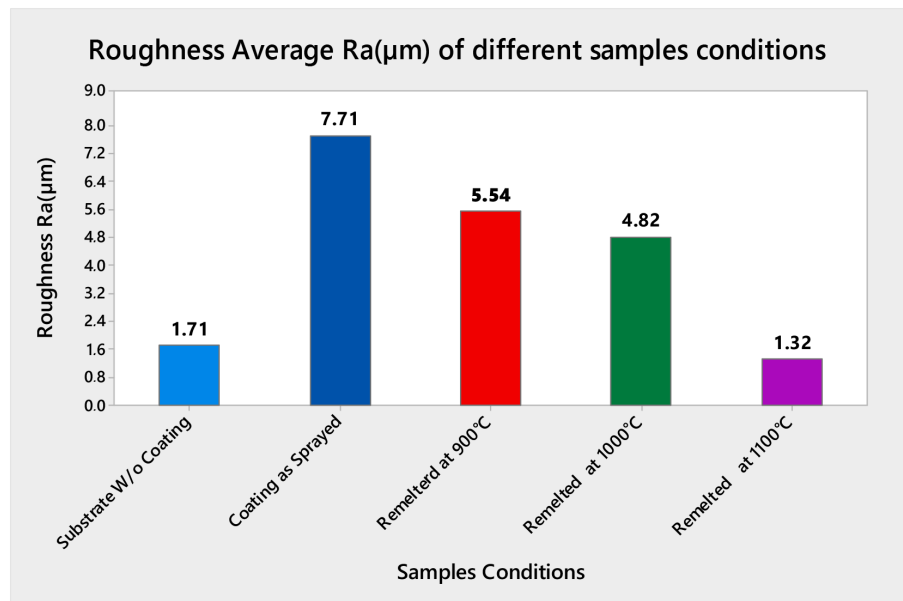


Figure 7. Average roughness for all sample conditions.

Table 5. Area and wear volume loss method determined by the Linearly Reciprocating Ball-on-Flat Sliding Test and calculation according to the standard ASTM G133-05(2016) (data from Ref. [20]).

Sample/Coating Condition	Wear Track Profile Area (mm ²)	Length of Sliding Stroke (mm)	Calculated Lost Wear Volume (mm ³)
As-Sprayed	1.41	10	14.1
Remelted at 900 °C	0.51	10	5.1
Remelted at 1000 °C	0.44	10	4.4
Remelted at 1100 °C	0.36	10	3.6

3.4. Roughness Measuring Results

Figure 7 shows the average roughness of each sample surface. The APS process worsens the surface roughness of the samples. However, the remelting process significantly improves it due to the densification of the coatings, which improves the coating's topography.

3.5. Microhardness Results

Figure 8 presents the average microhardness for each coating condition. In each microhardness graph, each point is 25 µm apart from the others and represents the average of five indentations taken every 5 µm. The values shown in Figure 8 pertain specifically to the coating region under different conditions: as-sprayed, remelted at 900, 1000, and 1100 °C, with standard deviations of 54.6, 52.0, 42.9, and 28.2 HV_{0.5}, respectively. The microhardness values for the interface region between the substrate and coating, influenced by the diffusion of the coating material into the substrate as well as the substrate values, are shown in Figure 9.

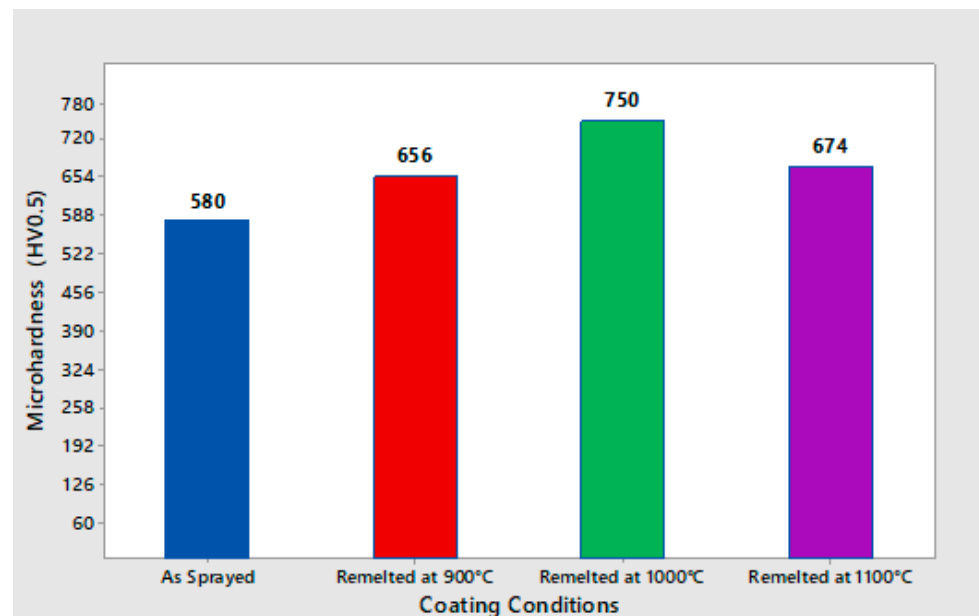


Figure 8. Average microhardness for all coating conditions.

The as-sprayed, remelted at 900 °C, and remelted at 1000 °C coatings exhibited increasing microhardness, influenced by the remelt temperature. However, decreased microhardness was observed for the coating sample remelted at 1100 °C. The most likely reason for such a decrease is the range of heat temperature for remelting and the cooling range of both the initial temperature and time that can permit more pronounced grain growth, which led to the decreasing hardness [21]. Figure 10 presents the microhardness profiles of the coatings, in which the microhardness varies according to the coating condition. The curve with the smallest variation is the curve of the remelted coating at 1100 °C, which verifies that this coating is denser and its microstructure is more homogeneous.

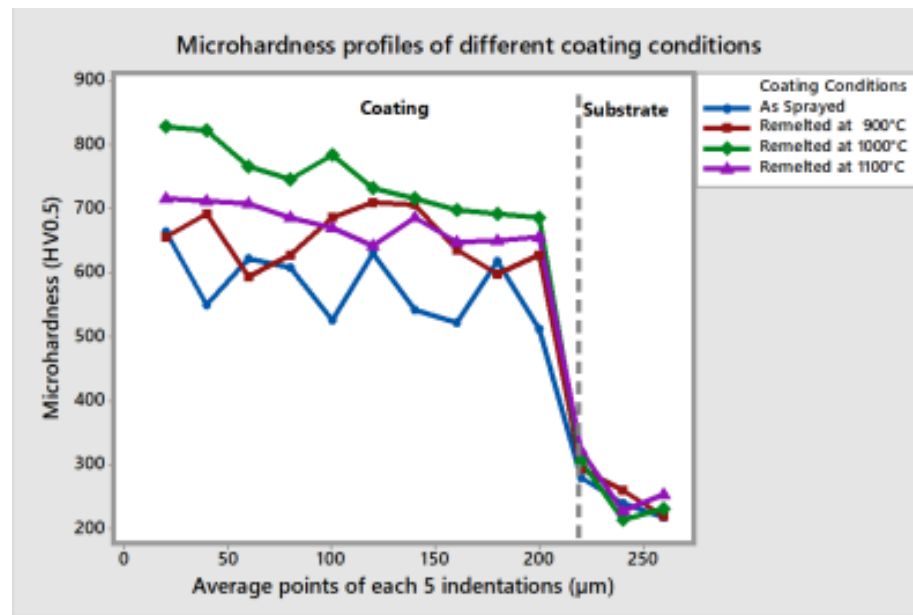


Figure 9. Average microhardness profiles for all coating conditions.

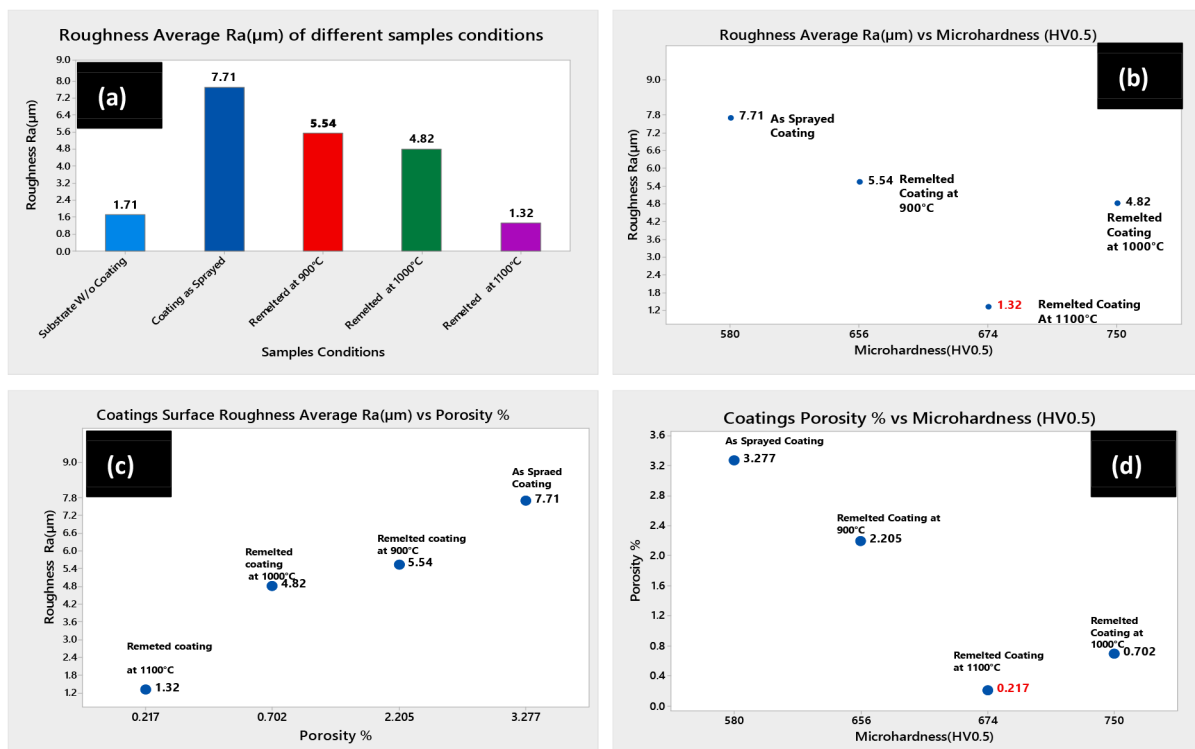


Figure 10. Overview of correlated obtained results. (a) Roughness average for all samples' conditions, (b) correlation between roughness average Ra (µm) and microhardness (HV_{0.5}), (c) correlation between roughness average Ra (µm) and porosity %, (d) correlation between porosity % and microhardness (HV_{0.5}).

3.6. Quantitative Results Relationship

Figure 10 presents and consolidates some relevant quantitative results. Figure 10b shows the relationship between roughness and microhardness; note that the greater the roughness, the lower the microhardness. Figure 10c indicates the relationship between the roughness and porosity, where the lower the porosity, the lower the roughness. Finally, Figure 10d presents the relationship between porosity and microhardness, where the greater

the porosity, the lower the microhardness. Table 6 provides all coating conditions and the main quantitative data related to them.

Table 6. Overview of the main quantitative results.

Coating Condition	Wear Track Profile (mm ²)	Lost Wear Volume (mm ³)	Wear Rate [mm ³ /(Nm)]	Porosity Coating Area %	Roughness Average Ra (μm)	Microhardness Average (HV _{0.5})
As Sprayed	1.41	14.1	9.16×10^{-5}	3.28	7.71	580
Remelted at 900 °C	0.51	5.1	7.46×10^{-5}	2.21	5.54	656
Remelted at 1000 °C	0.44	4.4	5.97×10^{-5}	0.70	4.82	750
Remelted at 1100 °C	0.36	3.6	4.10×10^{-5}	0.22	1.32	674

4. Conclusions

The results obtained in this work allow the following conclusions:

- The remelting process is a basic requirement to obtain the best performance of nickel-based self-fluxing coatings deposited by atmospheric plasma spraying.
- The remelting temperature strongly influences the tribological properties of the coatings.
- The results obtained in this research evidenced and confirmed that for this nickel-based self-fluxing alloy, the remelting temperature limit in a controlled-atmosphere furnace to obtain excellent tribological properties is 1100 °C.
- The remelting process and temperature level drastically influence the porosity percentage of the coating. The porosity percentage of remelted coating at 1100 °C is around 15 times less than the as-sprayed coating.
- The coefficient of friction of the remelted coating at 1100 °C was lower and more stable than the other coatings conditions, which suggested that this coating was smoother, denser, and more homogeneous than the other coatings.
- The wear rate of the remelted coating at 1100 °C was 2.23 times lower than the as-sprayed coating.
- The lost wear volume of the remelted at 1100 °C coating was 3.92 times lower than the as-sprayed coating.
- In general, thermal spraying worsens roughness; however, after remelting at 1100 °C, the roughness of this coating is 30% better than the roughness of the substrate and 5.8 times lower than the as-sprayed coating.
- The highest microhardness of a remelted coating in this research is 2.5 times greater than the substrate.
- The coating porosity influences inversely the microhardness and directly the coating roughness.
- Upon increasing the coating roughness, the microhardness tends to decrease.

Author Contributions: Methodology, F.C.M. and F.R.C.; Formal analysis, F.E.F. and A.A.C.; Investigation, F.C.M.; Resources, M.M.; Data curation, A.A.C.; Writing—original draft, F.C.M.; Writing—review & editing, C.R.C.L.; Visualization, A.A.; Supervision, C.R.C.L.; Project administration, M.M.; Funding acquisition, M.M. All authors have read and agreed to the published version of the manuscript.

Funding: This research was partially funded by CAPES-PRINT, grant 88881.310340/2018-01.

Data Availability Statement: The raw data supporting the conclusions of this article will be made available by the authors on request.

Acknowledgments: The authors acknowledge Stony Brook University for assistance and support in obtaining the coatings and Anton Paar for their support in carrying out the tribological tests. Francisco Monção would like to thank Mackenzie Presbyterian University and Mackenzie Presbyterian Institute for the scholarship during the doctorate.

Conflicts of Interest: Author Filipe E. Freitas was employed by the company Anton Paar do Brasil Ltda. The remaining authors declare that the research was conducted in the absence of any commercial or financial relationships that could be construed as a potential conflict of interest.

References

1. Kornienko, E.E.; Lapushkina, E.J.; Kuzmin, V.I.; Vaschenko, S.P.; Gulyaev, I.P.; KartaeV, E.V.; Sergachev, D.S.; Kashapov, N.; Sharifullin, S.; Fayrushin, I. Air Plasma Sprayed Coatings of Self-Fluxing Powder Materials. *J. Phys.* **2014**, *567*, 012010. [[CrossRef](#)]
2. Schanner, J.; Funke, R.; Schubert, A.; Hasse, A. Investigating the Friction Behavior of Turn-Milled High Friction Surface Microstructures under Different Tribological Influence Factors. *J. Manuf. Mater. Process.* **2022**, *6*, 143. [[CrossRef](#)]
3. Zum-Gahr, K.H. *Microstructure and Wear of Materials*, 1st ed.; Tribology Series 10; Elsevier: Amsterdam, The Netherlands, 1987.
4. Kato, K.; Hokkirigawa, K. An experimental and theoretical investigation of ploughing, cutting and wedge formation during abrasive wear. *Tribol. Int.* **1988**, *21*, 51–57.
5. Holmber, K.; Ali, E. Global Impact of Friction on Energy Consumption, economy, and environment. *FME Trans.* **2012**, *47*, 221–234.
6. Jost, H.P. *Tribology: Origin and Future*; International Tribology Council: London, UK, 1966.
7. Nunes, M.M.; da Silva EMRengetti, R.A.; Brito, T.G. Analysis of Quenching Parameters in AISI 4340 steel by Using Design of Experiment. *Mater. Res.* **2019**, *22*, e20180315. [[CrossRef](#)]
8. Sang, Y.; Sung, G.; Liu, J. A 4340 steel with Superior Strength and Toughness Achieved by Heterostructure via Intercritical Quenching and Tempering. *Metals* **2023**, *13*, 1139. [[CrossRef](#)]
9. Jami, M.; Gil, E.; Ushiña, E.; Cabrera, V.H.; Cartagena, A. Determina hardness and torsional resistance of AISI/SAE 4340 Steel, treated by quenching at 860 °C and tempering at 300 °C, 350 °C and 400 °C. *Mater. Proc.* **2022**, *49*, 35–42.
10. Chi, Y.C.; Lee, S.; Cho, K.; Duffy, J. The effects of tempering and test temperature on the dynamic fracture initiation behavior of an SAE 4340 VAR steel. *Mater. Sci. Eng. A* **1989**, *114*, 105–126. [[CrossRef](#)]
11. Lim, N.S.; Bang, C.W.; Das, S.; Jin, H.W.; Ayer, R.; Park, C.G. Influence of tempering temperature on both the microstructural evolution and elemental distribution in SAE 4340 steels. *Met. Mater. Int.* **2012**, *18*, 87–94. [[CrossRef](#)]
12. Lee, W.-S.; Su, T.-T. Mechanical properties and microstructural features of SAE 4340 high-strength alloy steel under quenched and tempered conditions. *J. Mater. Process. Technol.* **1999**, *87*, 198–206. [[CrossRef](#)]
13. Totten, G.E. *Steel Heat Treatment: Metallurgy and Technologies*, 2nd ed.; CRC: Portland, OR, USA, 2007; 833p.
14. Martin, D.T.; Rad, M.Z.; Macdonald, A.; Hussain, T. Beyond Traditional Coatings, a review on Thermal Sprayed and Smart coatings. *J. Therm. Spray Tech.* **2019**, *28*, 598–644. [[CrossRef](#)]
15. Fotovvati, B.; Namdari, N.; Dehghanghadikolaei, A. On Coating Techniques for Surface Protection: A Review. *J. Manuf. Mater. Process.* **2019**, *3*, 28. [[CrossRef](#)]
16. Simunovic, K.; Havrlisan, S.; Saric, T.; Vukelic, D. Modeling and Optimization in Investigating Thermally Sprayed Ni-Based Self-Fluxing Alloy Coatings: A Review. *Materials* **2020**, *13*, 4584. [[CrossRef](#)]
17. Dong, X.Y.; Luo, X.T.; Ge, Y.; Li, C.J. Enhancing the hot-corrosion resistance of atmospheric plasma sprayed Ni-based coatings by adding a deoxidizer. *Mater. Des.* **2021**, *211*, 110154. [[CrossRef](#)]
18. McGinty, B.M.; Craven, P. *5 Opportunities of Circular Economy*; World Resource Institute: Washington, DC, USA, 2021.
19. Viswanathan, V.; Katiyar, N.K.; Goel, G.; Matthews, A.; Goel, S. Role of thermal spray in combating climate change. *Emergent Mater.* **2021**, *4*, 1515–1529. [[CrossRef](#)]
20. Kazamer, N.; Murtean, R.; Vă, P.C.; Pascal, D.T.; Mărginean, G.; Serban, V.A. Comparison of Ni-Based Self-Fluxing Remelted for Wear and Corrosion Applications. *Materials* **2021**, *14*, 3293. [[CrossRef](#)]
21. *ASTM G133-05*; Standard Test Method for Linearly Reciprocating Ball-on-Flat Sliding Wear. ASTM International: West Conshohocken, PA, USA, 2016.
22. Bergant, Z.; Trdan, U.; Grum, J. Effect of high-temperature furnace treatment on the microstructure and corrosion behavior of NiCrBSi flame-sprayed coatings. *Corros. Sci.* **2014**, *88*, 372–386. [[CrossRef](#)]
23. Kim, H.J.; Hwang, S.Y.; Lee, C.H.; Javanon, P. Assessment of wear performance of flame Sprayed and fused Ni-based coating. *Surf. Coat. Technol.* **2003**, *172*, 262–269. [[CrossRef](#)]
24. Li, C.J.; Luo, X.T.; Dong, X.Y.; Zhang Li Li, C.X. Recent Research Advances in Plasma Spraying of Bulk- like Dense Metal Coatings with Metallurgically Bonded Lamellae. *J. Therm. Spray Tech* **2022**, *31*, 5–27. [[CrossRef](#)] [[PubMed](#)]
25. Odhiambo, G.J.; Li, W.G.; Zhao, Y.T.; Li, C.L. Porosity, and Its Significance in Plasma Sprayed Coating: A Review. *Coating* **2019**, *9*, 460. [[CrossRef](#)]
26. Yang, L.; Ma, W.; Gao, F.; Xi, S. Effect of Groove Width on Micromachine Groove Texture Tribology Characteristics of 0Cr17Ni7Al. *Coatings* **2022**, *12*, 12121. [[CrossRef](#)]
27. Huang, S.; Zhou, J.; Sun, K.; Yang, H.; Cai, W.; Liu, Y.; Zhou, P.; Wu, S.; Li, H. Microstructural Characteristics of Plasma Sprayed NiCrBSi coatings and Their Wear and Corrosion Behavior. *Coatings* **2021**, *11*, 170. [[CrossRef](#)]
28. Sousa, J.M.S.; Silva, R.G.N.; Pereira, A.S.P.; Amaral, C.; Pereira, M. Effect of Laser Remelting on Tribological Performance of Ni-Cr-B-Si Coatings Deposited by Laser Metal Deposition. *Soldag. Inspeção* **2020**, *25*, e2515. [[CrossRef](#)]

29. Ndumia, J.N.; Kang, M.; Li, J.; Liu, J.; Li, H. Influence of Heat Treatment on the Microstructure and Wear properties of Arc-Sprayed FeCrAl/Al Coating. *Coatings* **2022**, *12*, 374. [[CrossRef](#)]
30. Muntean, R.; Vălean, P.C.; Kazamer, N.; Utu, I.D.; Mărginean, G.; Serban, V.A. Effect of Feedstock Powder Intrinsic Characteristics on the Tribological Behavior of Inductively Remelted NiCrBSi Flame-Sprayed Coatings. *Lubricants* **2023**, *11*, 363. [[CrossRef](#)]

Disclaimer/Publisher's Note: The statements, opinions and data contained in all publications are solely those of the individual author(s) and contributor(s) and not of MDPI and/or the editor(s). MDPI and/or the editor(s) disclaim responsibility for any injury to people or property resulting from any ideas, methods, instructions or products referred to in the content.